Received: 18 October 2017 | Revised: 30 May 2018 | Accepted: 31 May 2018 | Uncorrected manuscript published: 4 June 2018

DOI: 10.1111/tra.12583

WILEY Traffic

ORIGINAL ARTICLE

Engaging myosin VI tunes motility, morphology and identity in endocytosis

Michael Ritt | Sivaraj Sivaramakrishnan

Department of Genetics, Cell and Developmental Biology, University of Minnesota, Minneapolis, Minnesota

Correspondence
Sivaraj Sivaramakrishnan, Department of Genetics, Cell and Developmental Biology, University of Minnesota, Minneapolis, MN 55455.
Email: sivaraj@umn.edu

Funding information
National Institute of General Medical Sciences, Grant/Award Number: 1-R35-GM126940-01; NIH Office of the Director, Grant/Award Number: 1DP2 CA186752-01

While unconventional myosins interact with different stages of the endocytic pathway, they are ascribed a transport function that is secondary to the protein complexes that control organelle identity. Endosomes are subject to a dynamic, continuous flux of proteins that control their characteristic properties, including their motility within the cell. Efforts to describe the changes in identity of this compartment have largely focused on the adaptors present on the compartment and not on the motile properties of the compartment itself. In this study, we use a combination of optogenetic and chemical-dimerization strategies to target exogenous myosin VI to early endosomes, and probe its influence on organelle motility, morphology and identity. Our analysis across timescales suggests a model wherein the artificial engagement of myosin VI motility on early endosomes restricts microtubule-based motion, followed by morphological changes characterized by the rapid condensation and disintegration of organelles, ultimately leading to the enhanced overlap of markers that demarcate endosomal compartments. Together, our findings show that synthetic engagement of myosin VI motility is sufficient to alter organelle homeostasis in the endocytic pathway.

KEYWORDS

chemical dimerization, early endosomes, endocytosis, molecular motors, optogenetics, synthetic biology, unconventional myosins

1 | INTRODUCTION

Endocytosis is a dynamic process that relies on the continuous flux of proteins through membrane compartments, on a timescale of tens of minutes. While unconventional myosins have been implicated in endocytosis,[1] their motile function at different stages of the endocytic pathway remains poorly understood.[2] In contrast to microtubule-based motors that drive super-diffusive movement within cells along linear, unbranched microtubules, unconventional myosins navigate a mesh-like actin cytoskeleton.[3] Unconventional myosin motility is therefore more conducive for short-range transport and occurs at speeds that can be an order of magnitude slower than microtubule traffic.[4] Consequently, unconventional myosins are unlikely to serve primarily as transporters in endocytosis. In fact, targeting myosins to subcellular scaffolds has been shown to reduce their diffusive motion, presumably by linking them to the surrounding actin cytoskeleton.[5] Hence, this study is designed to address alternate roles for unconventional myosin motility in cells.

Myosin VI is an unconventional myosin that is targeted by different cargo adaptors to distinct stages of the endocytic pathway.[6] In addition, myosin VI is the only minus-end-directed actin-based motor[7,8] and therefore is uniquely positioned to direct the motion of endocytic vesicles toward the cell interior within the polarized actin cortex. Myosin VI can bind directly to clathrin[9] and Dab2[10–12] leading to its localization in clathrin-coated pits. Subsequently, myosin VI is recruited to uncoated vesicles lacking clathrin through interactions with the uncoated vesicle marker GIPC.[13,14] Myosin VI localization has been shown to persist through early endosomes,[15] a compartment demarcated by the presence of Rab5a.[16] Myosin VI interaction with LMTK2 on early endosomes is important for endosome recycling to the plasma membrane.[15] Despite the confirmed localization of myosin VI to multiple stages of the endocytic pathway, a direct role for myosin VI in membrane traffic remains poorly characterized, in part due to the motility of endosomes within the cytosol being associated primarily with the microtubule network.[6] Hence, we focus here on

elucidating the effects of myosin VI motility on the early endocytic pathway using synthetic adaptors.

Two different approaches have been used to synthetically engage molecular motors to subcellular scaffolds. The first utilizes the formation of chemically inducible dimers between FKBP and FRB upon the addition of rapamycin or rapalogs.[17–20] The second leverages the well-established optogenetic pairs of (frequently, ePDZ1b and LOV2—though others have been used[21–23]) to trigger reversible dimerization using light stimulation.[24,25] These techniques have been extensively used to control organelle positioning and explore actin/microtubule motor competition. However, the long-term consequences of motor engagement and myosin biology on organelle homeostasis are unclear. In this study, we use a combination of these techniques to study the functional consequences of synthetic engagement on cellular cargo.

Given the constant flux of proteins through distinct membrane compartments during endocytosis, we anticipate that engagement of myosins will lead to immediate changes in motility and localization of vesicles that in turn can gradually shift the dynamic equilibrium of constituents of the entire pathway. To examine the effects at multiple timescales, we employ a combination of acute optogenetic engagement (seconds-minutes) and a sustained chemical recruitment of myosin VI to early endosomes (approximately hours) to link biophysical measurements of myosin motility to functional redistribution of endocytic traffic. Using optogenetic labeling, we observed that on short and intermediate timescales (3-10 minutes), myosin VI was able to influence the motile properties of endocytic traffic as well as the morphology of individual organelles. Prolonged interaction (4-8 hours) between myosin VI and endosomes was observed to dramatically change both the morphology and identity of the compartment as judged by colocalization with late endosomal and lysosomal markers. In spite of the changes induced by myosin VI recruitment, the reorganized compartment was still able to interact with the normal endocytic pathway as demonstrated by transferrin uptake. Furthermore, the extent of the observed change in morphology was found to be dependent on the directionality of the motor. Together, our findings suggest that the unique properties of unconventional myosin motility can alter the progression of organelle homeostasis in the endocytic pathway through synthetic coupling that, over time, changes the motility, morphology and identity of these compartments.

2 | RESULTS

2.1 | Optogenetic engagement of myosin VI to early endosomes alters both motility and morphology

To examine the immediate effects of myosin VI motility on endocytic vesicle morphology and function, we utilized a previously characterized optogenetic system (ePDZb1/LOV)[24,26] to label target cargo with myosin VI-green fluorescent protein (GFP) fusion constructs in a light-dependent manner (Figure 1A). This myosin VI is artificially dimerized by a leucine zipper-containing GCN4 motif and contains the light-activated LOV domain in place of the cargo-binding domains of myosin VI. Upon light activation, myosin VI is targeted to cargo by a fusion protein that contains the binding partner for the optogenetic system (ePDZb1) and a localization motif for Rab5 early endosomes. After light stimulus, we observed labeling of the early endosome compartment immediately after light activation that subsequently stabilizes on the order of seconds (Figure 1B, representative data).

Individual endosomes were tracked before and after light stimulation, and changes in the profiles of the time-correlated mean-squared displacement (MSD) of each endosome were measured (Figure 1C,D, representative data). Time-correlated MSDs are plotted relative to the time at which each endosome is first observed (as opposed to a "delay time" normalized to zero) allowing differences over time to be explored. To understand the effect of myosin engagement on the movement of organelles, we compared the average slope of individual traces before (pre) and after (post) stimulation to cells not exposed to light stimulation (pre and post are determined by the halfway point of each movie). The heterogeneity in movement across endosomes necessitated a pairwise comparison of the pre and post segments of individual endosomes. Therefore, only trajectories that appear before stimulation and persist after stimulation were selected for quantitative analysis. Trajectories were classified into 2 categories based on either an increase (positive slope change) or decrease (negative slope change) in the average slope of their MSD trace following stimulation (Figure 1C,D, representative data). Traces with decreasing (negative) slopes are "slowing down" as compared to traces with increasing (positive) slopes. Given the broad distribution of average slope of the MSD profile of individual traces, cumulative distribution functions (CDFs) were used to evaluate changes across the endosome population (Figure 1E, $n \geq 6$ cells per condition). Particularly evident was a decrease in the overall number of traces with high average slopes after light stimulation (as compared to cells not stimulated with light over the same amount of time) (Figure 1F, green lines). Comparing the fraction of MSD traces per cell that experience a decrease in their slopes after stimulation, cells that are stimulated have a significantly higher proportion of endosomes that are slowing down after stimulation (Figure 1G, combined data, $n \geq 6$ cells per condition). Localization of a truncated myosin VI, containing only the motor's lever arm, was unable to cause similar changes (Figure S1 in File S1, Supporting Information).

This apparent slowdown in motility was also observed over intermediate timescales (Figure 2, Movies S1 and S2). Representative sequential 60-second time-lapses of cells are displayed in Figure 2A,C using a temporal color code (scale shown in Figure 2A). Motility before light stimulation looked similar to motility in cells which were not stimulated (Figure 2C, red box). However, after stimulation, particles in stimulated cells lose the strong linear directed motion evident in cells not stimulated with light (compare: Figure 2B,D). In addition, some endosomes in stimulated cells were observed to change morphology (condensation and disintegration of individual puncta) as compared to endosomes in cells that were not stimulated with light (Figure 2C, cyan circle; Movies S1 and S2).

While we have been observing actin-based motors' effects on endocytosis, endocytic traffic is predominantly observed on the microtubule network[27] (Figure S2A-C in File S1). To test whether the changes in organelle morphology and identity that we have observed are due to combined effects of microtubule motors and myosin VI, we

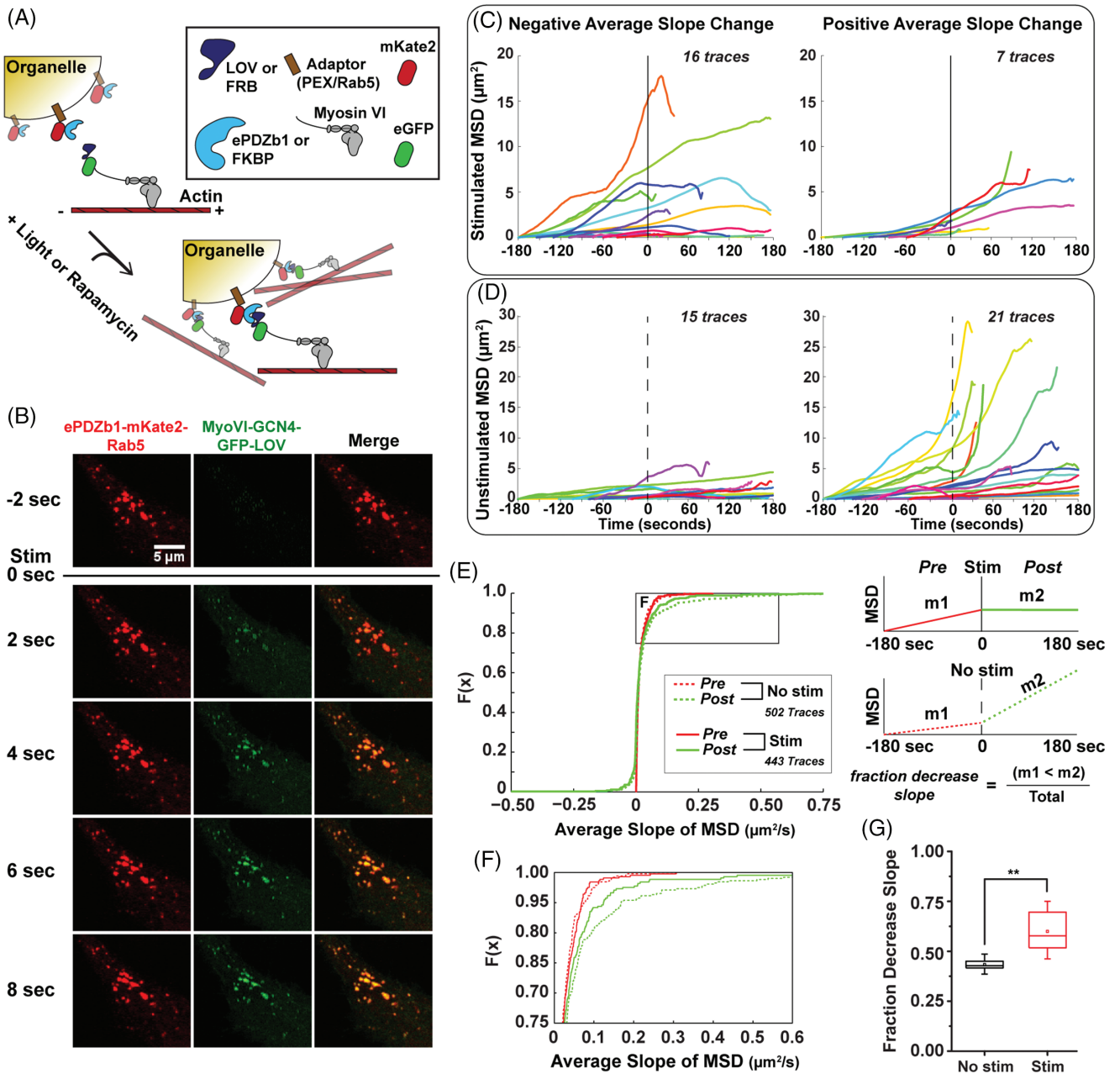

FIGURE 1 Optogenetic control of cargo-motor interaction alters cargo motility. (A) Schematic of elements used in experiments. Two sets of coupling partners (ePDZb1/LOV—short timescales; FKBP/FRB—long timescales) are used to monitor the effects of motor engagement to vesicular organelles over time using confocal fluorescence microscopy in cells. (B) Time-lapse series of representative images showing optogenetic localization of Rab5-mKate2 labeled early endosome compartments with myosin VI-GCN4-GFP in HeLa cells. Optogenetic stimulation with 488 nm laser at the indicated time point (Stim) drives rapid myosin VI recruitment to Rab5 endosomes that increases toward saturation on a scale of seconds. (C-F) MSD plots of Rab5 early endosome motion for a region of interest from representative stimulated (C), and not stimulated (D) cells. These plots have been adjusted for time correlation so that profiles are plotted relative to the time that they are first observed. MSD plots are separated by whether there is a negative change (C, D—left panel) or a positive change (C, D—right panel) in the average slope of each MSD trace after stimulation. Vertical black lines denote the start of light stimulation. For cells that were not stimulated with light, an arbitrary frame corresponding to the same amount of time is chosen for the purpose of analysis denoted by the vertical dashed lines. (E) Plot of the CDF of the average slope of the MSD traces before (red) and after (green) stimulation ($n \geq 6$ cells per condition, >10 MSD trace slopes per cell, total number of traces indicated in key). Schematic shows time course of experiment and indicates how data are grouped. (F) Callout from CDF presented in (E). (G) Box and whisker plots comparing the average fraction of trajectories with decreasing slopes after stimulation ($n \geq 6$ cells per condition). Top and bottom hashes are 95th and 5th percentiles, box is 75th and 25th percentiles, line is median and middle spot is mean. Significance assessed by Student's *t* test: $^{**}P < .01$

treated cells with nocodazole to depolymerize the microtubule network. The toxicity of depolymerizing the microtubule network prevents observing long-term (approximately hours) changes in organelle morphology. Therefore, we characterize the short-term (approximately minutes) changes in motility using the optogenetic system. In nocodazole-treated cells prior to stimulation, endosomes were largely

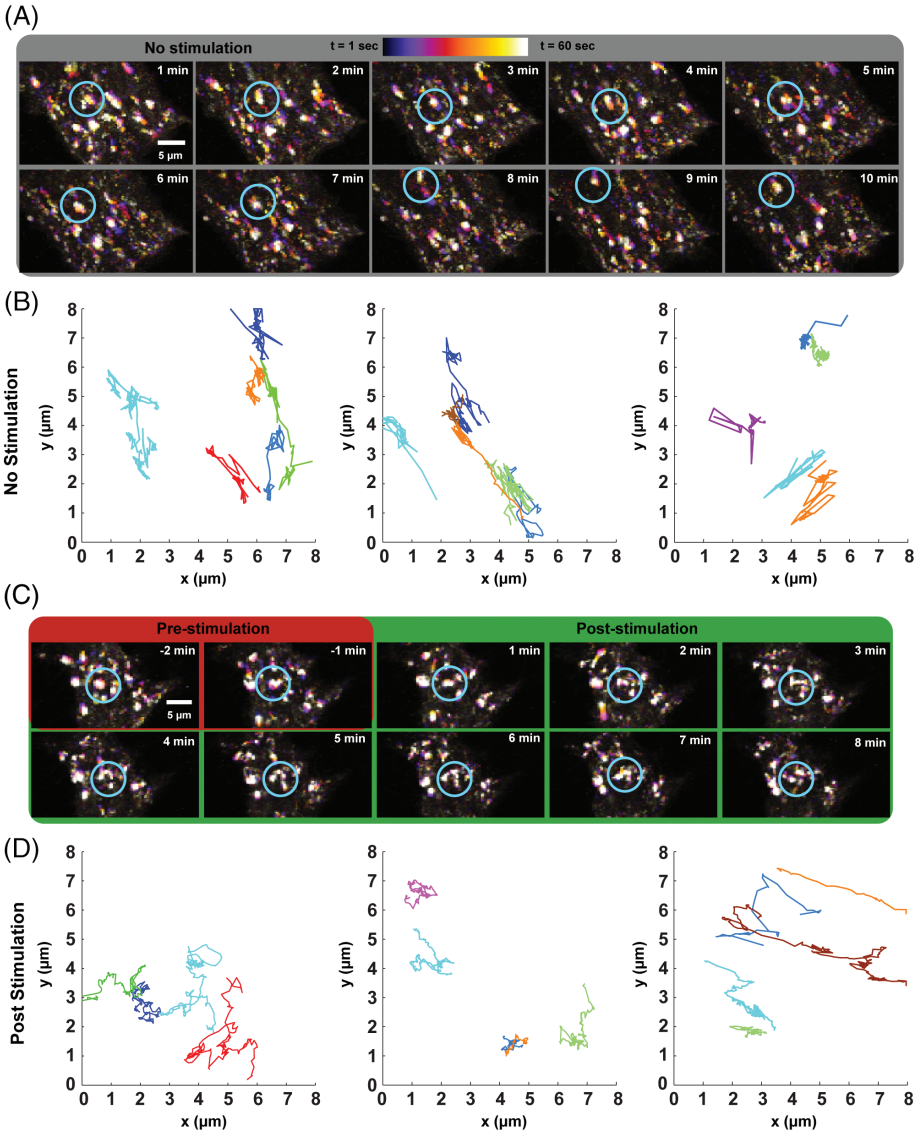

FIGURE 2 Optogenetically labeled endosome cargo displays changes in motility over intermediate timescales. (A, C) Temporal color code of 60-second time-lapses of Rab5 endosomes in a region of interest in cells that were not stimulated (A; Movie S1) and optogenetically stimulated (C; Movie S2) HeLa cells. After stimulation (C, green box), motility loses the strong directional movement observed in (A) and in prestimulated cells (C, red box). A representative endosome in each image series is marked by a cyan circle. (B, D) Trajectories of labeled endosomes in an 8 × 8 μm region of interest from 3 individual cells after light stimulation (duration: ~8 minutes) (D) or for an equivalent amount of time in cells that were not stimulated (B)

stationary (Figure 3A, red box, Movie S3). However, after light stimulation, endosomes began to move (Figure 3A, green box, Movie S3; Figure 3B). This increase in motility after stimulation was evident by comparing the average MSD of the endosomes in a cell before and after light stimulation (Figure 3C, representative data). Comparing the average slopes of MSDs of cells that were not light stimulated to those of stimulated cells before and after stimulation (or an equivalent amount of time in cells that were not stimulated) revealed an increase in the population of MSD traces with a high rate of change in stimulated cells as compared to cells that were not stimulated (Figure 3D). Comparing nocodazole-treated cells after stimulation to untreated cells after stimulation, the population of slopes was not substantially different, suggesting that the motility observed was largely independent of the activity of microtubule motors. In fact, by observing endosomes on longer timescales, similar changes in motility and morphology are observed following nocodazole treatment (Figure 3B), as was seen in untreated cells (Figures 2D and 3D, bottom). This suggests that dynamic reshaping of the endocytic compartment can be caused by the motile properties of myosin VI independently of microtubule-based motors.

2.2 | Long-term engagement of myosin VI to organelles changes their cellular organization

While optogenetics allows us to observe the influence of myosin motility on organelle morphology over a period of minutes, an orthogonal approach is necessary to investigate the influence of myosin engagement over longer timescales (approximately hours). To overcome this, our fusion proteins were adapted to use the FKBP-FRB rapamycin-inducible dimerization system in place of optogenetic

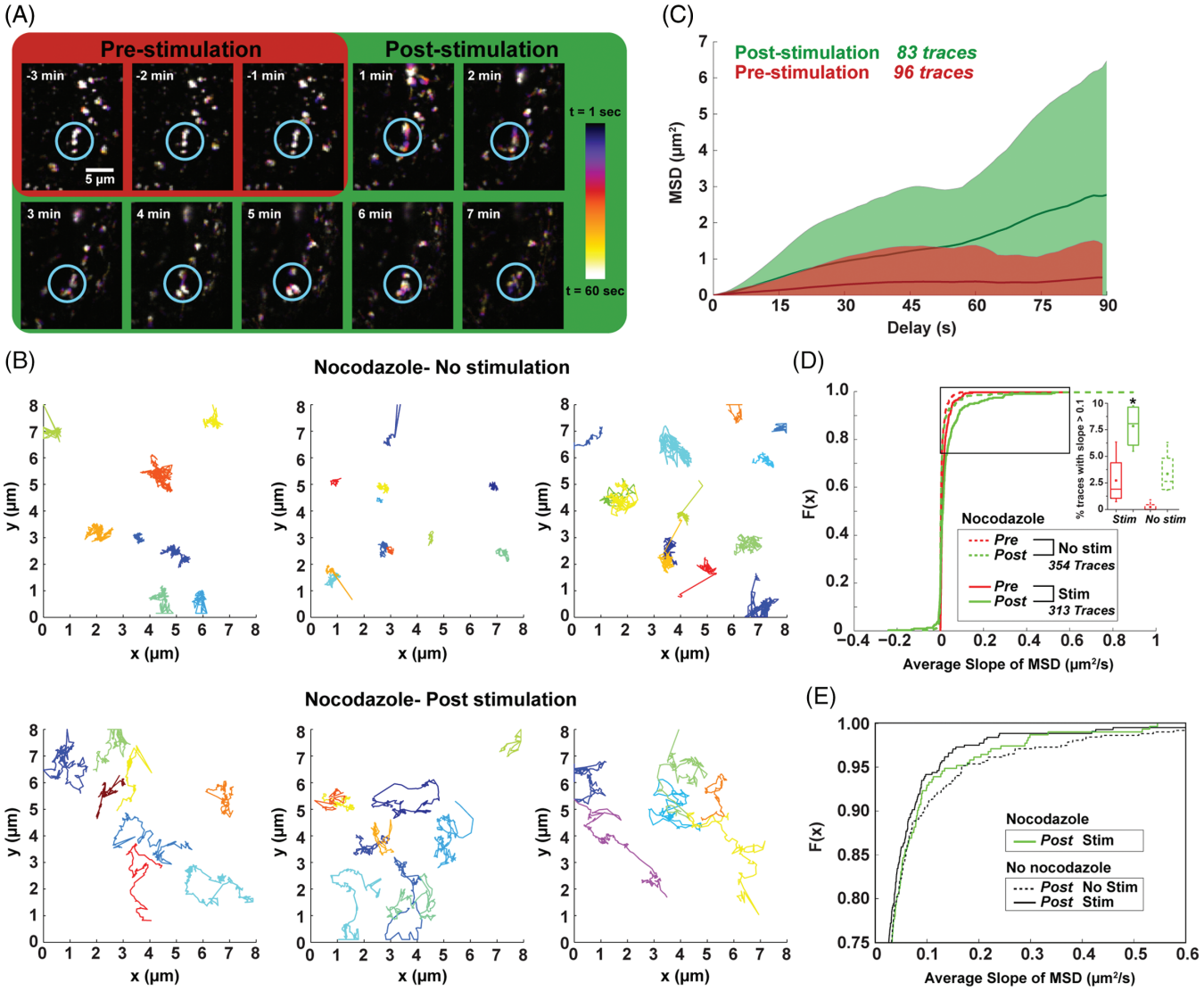

FIGURE 3 The microtubule network is not necessary for the altered motility directed by myosin VI. (A) Temporal color code of 60-second time-lapses of Rab5 endosomes in nocodazole-treated HeLa cells before (red box; Movie S3) and after (green box; Movie S3) optogenetic stimulation. Motility is not observed before stimulation. A representative endosome is marked by a cyan circle. (B) Trajectories of endosomes in an 8 × 8 μm regions of interest in 3 different cells treated with nocodazole, without stimulation (top) or after light stimulation (bottom) (duration: ~8 minutes). (C) Representative average MSD plot for the nocodazole-treated cell depicted in (A) before (red) and after (green) stimulation. (D) CDF of the slopes of MSD traces of nocodazole-treated cells before and after stimulation. Cells that were not stimulated (dashed lines) are not exposed to light, instead an arbitrary frame corresponding to the same amount of time is chosen for the purpose of analysis. Inset: percentage of traces per cell before and after stimulation that have an average slope greater than 0.1 $\mu m^2/s$ (n = 4 cells per condition). (E) The indicated region of the CDF plot in (D) is displayed below the full plot and displays the CDF for poststimulation slopes in nocodazole-treated cells (green), untreated cells without stimulation (black dashed) and untreated cells with stimulation (black). ($n \geq 4$ cells per condition; total number of traces analyzed indicated in figure key). For box and whisker plots: top and bottom hashes are 95th and 5th percentiles, box is 75th and 25th percentiles, line is median and middle spot is mean. Significance assessed by Tukey's range test. *$P < .05$

triggering (Figure 1A). To test the efficacy of this system, we first utilized this system with peroxisomes (a non-native, but stable and tractable organelle) as cargo, as has been reported by other groups.[17–20,24,25] Labeling of peroxisomes was observed within 1 hour of rapamycin (100 nM) addition (Figure 4A,B). Over the course of 4 hours, rapamycin-triggered myosin VI labeling of peroxisomes increased significantly compared to untreated cells, with a further slight increase after 4 more hours (8 hours total, Figure 4C).

While it has been observed that both monomers and dimers of myosin VI are capable of interacting with cargo in vitro, the physiological roles of these 2 states are unclear. To help address this, we labeled peroxisomes with either monomeric or dimeric (GCN4) myosin VI and observed the resulting morphology of the cargo (Figure 4D-G). While both monomeric and dimeric myosin VI label peroxisomes effectively, dimeric myosin VI caused a dramatic decrease in the apparent number of peroxisomes whereas monomeric myosin VI causes a statistically insignificant average decrease (Figure 4H). In addition, looking at the total population of peroxisomes across all cells, there was an increase in the number of very large or tightly clustered peroxisomes in cells where peroxisomes were labeled with dimeric myosin VI as compared to untreated cells (Figure 4I). Furthermore, this shift in apparent size was not observed for cells with

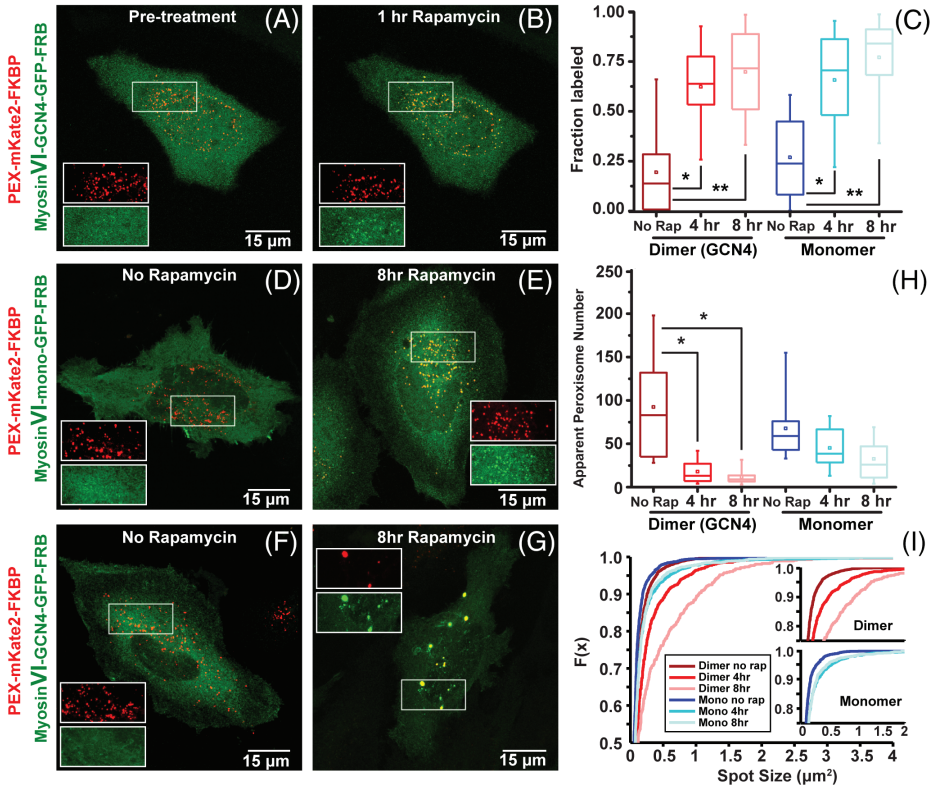

FIGURE 4 FKBP/FRB-mediated cargo-motor interaction allows changes in morphology to be monitored over long timescales. (A, B) Rapamycin-triggered localization of myosin VI-GCN4-GFP-FRB to peroxisomes labeled with PEX3-mKate2-FKBP in HeLa cells. Prior to treatment (A), myosin VI-GCN4-GFP localization is diffuse; however, after 1 hour of treatment, (B) colocalization of myosin with peroxisomes is observed. (C) Box and whisker plots of the fraction of peroxisomes co-labeled with either myosin VI-GCN4-GFP-FRB or myosin VI-monomer-GFP-FRB and PEX3-mKate2-FKBP after 100 nM rapamycin treatment at the indicated times ($n \geq 3$ repeats of at least 12 cells per condition). (D-G) Effects of myosin VI labeling on peroxisome morphology after 8 hours when labeled with a monomeric myosin VI (D, E) or a dimeric (GCN4) myosin VI (F, G). (H) Box and whisker plots of the apparent number of peroxisomes observed per cell in the indicated conditions. (I) CDF of the sizes of all detected peroxisomes in each of the conditions in (H). Insets are the top portion of the main CDF separated by myosin VI oligomeric state. Image insets are ×1.3 magnified and are presented at the same brightness contrast settings as the image from which they are taken. For box and whisker plots: top and bottom hashes are 95th and 5th percentiles, box is 75th and 25th percentiles, line is median and middle spot is mean. Significance assessed by Tukey's range test. *$P < .05$; **$P < .01$

peroxisomes labeled with monomeric myosin VI. The combination of the decrease in number and the increase in size or clustering observed with dimeric myosin VI suggests, at least superficially, that myosin VI motility may be causing peroxisomes to merge or associate closely, although other mechanisms may be possible.[28]

To probe whether there were similar effects on the more dynamic endocytic compartment, we returned to Rab5-labeled endosomes with the rapamycin-induced FKBP/FRB dimerization system (Figure 5A-D). Similar to the labeling of peroxisomes, we observed strong labeling of endosomes with myosin VI within 4 hours (Figure 5E). However, dimeric myosin VI showed a much greater variability in labeling as compared to monomeric myosin VI. Both endosomes labeled with dimeric myosin VI and those labeled with the monomer showed a decrease in the total area of the endocytic compartment (Figure 5F). Unlike similar changes for peroxisomes, the changes in endosome morphology do not depend on myosin oligomeric state. However, this observation may be influenced by the efficiency of labeling, as the more processive dimeric myosin VI did not label as efficiently as the monomeric myosin VI. As such, the molecular basis for the differential sensitivity of peroxisomes and early endosomes to the myosin oligomeric state remains unclear.

If the observed phenotypes resulted simply from increased motility, conjugation of cargo to a motor that walks in the opposite direction of myosin VI, but has largely similar motile properties, should have similar effects on cargo morphology. Myosin V, a motor which has been shown to roughly meet these specifications[29] was initially used to investigate this possibility. However, rapamycin-induced myosin V recruitment was comparatively poor and myosin V appeared to be primarily localized to the cell periphery, further complicating the analysis (Figure S3 in File S1). Instead, a myosin chimera previously characterized by Park et al[30] was used. This chimera (referred to here as myosin 6/5) fuses the motor domain of myosin VI to the lever arm of myosin V, preserving the motility of myosin VI, but with the directionality of myosin V. As with myosin VI, rapamycin treatment recruited the dimeric chimera robustly to endosomes (Figure 5G-I). However, labeling of Rab5 endocytic vesicles with myosin 6/5 did not result in a significant decrease in the total area of Rab5 (Figure 5J), suggesting that the minus-end-directed movement of myosin VI is essential for the changes in morphology. This finding is consistent with the role of myosin VI in several stages of the endocytic pathway.[31,32]

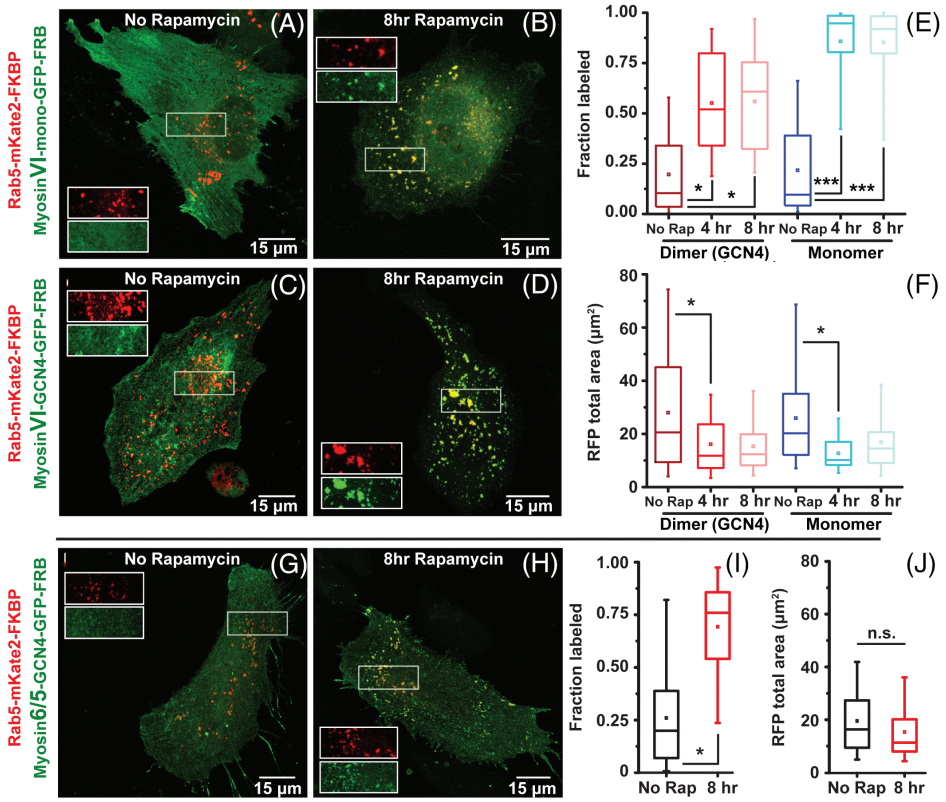

FIGURE 5 Rab5 early endosomes undergo a dramatic organizational shift when coupled to myosin VI but not a plus-end-directed myosin chimera. (A-D) Effects of myosin VI labeling on Rab5 early endosome morphology in HeLa cells after 8 hours of rapamycin treatment when labeled with a monomeric (A, B) or dimeric (C, D) myosin VI. (E) Fraction of Rab5 early endosomes labeled with either myosin VI-GCN4-GFP-FRB or myosin VI-monomer-GFP-FRB after 100 nM rapamycin treatment for the indicated times ($n \geq 3$ repeats of at least 12 cells each per condition). (F) Box and whisker plots of the total area of Rab5 endosomes per cell in the indicated conditions with myosin VI. (G, H) Effects of myosin 6/5 chimera-GCN4-GFP-FRB labeling on Rab5 early endosome morphology in untreated (G) and rapamycin-treated (H) HeLa cells after 8 hours. (I) Fraction of Rab5 early endosomes labeled with myosin 6/5 chimera-GCN4-GFP-FRB in untreated and 100 nM rapamycin-treated HeLa cells after 8 hours ($n \geq 3$ repeats of at least 12 cells each per condition). (J) Box and whisker plots of the total area of Rab5 endosomes per cell in the indicated conditions. Image insets are ×1.3 magnified and are presented at the same brightness contrast settings as the image from which they are taken. For box and whisker plots: top and bottom hashes are 95th and 5th percentiles, box is 75th and 25th percentiles, line is median and middle spot is mean. Significance assessed by Tukey's range test, $^{*}P < .05$; $^{***}P < .001$; n.s., not significant

2.3 | Myosin VI engagement alters the functional identity of early endosomes

To test whether the rearrangement of the endocytic compartment was still a functional part of the endocytic pathway, we monitored transferrin uptake by rapamycin-treated and untreated cells. In untreated cells after 10 minutes of transferrin uptake, transferrin is located within the early endocytic Rab5-labeled compartment (Figure S4A in File S1). Similarly, in spite of the observed decrease in total endocytic area, there is not a significant change in the amount of colocalization between transferrin and Rab5 in rapamycin-treated cells (Figure S4B,C in File S1), suggesting that the reorganized early endocytic compartment was still able to accept cargo. The recycling pathway containing Rab11,[33] however, was substantially altered by rapamycin treatment (Figure S4D-F in File S1). Because the cell is experiencing continual uptake of transferrin while in serum media, even during rapamycin treatment, it would be expected that if transferrin receptors were unable to traffic properly, they would deplete on the cell surface, and no further uptake would be possible. Contrary to this possibility, transferrin uptake is observed and can be seen to colocalize with Rab5 (Figure S4B in File S1) as well as Rab11 (Figure S4G,H in File S1, representative data). Based on this uptake, as well as the functional timescale of the reorganization (Figure S4I in File S1), we believe these reorganized endocytic compartments to be still functional.

To test whether the functional labeling of the early endocytic pathway had changed, we looked for markers for late endosomes (Rab7) and lysosomes (Lamp1) using fluorescent antibody staining. While there is a significant colocalization between early and late endosome markers in untreated cells, Rab7 showed a significant increase in colocalization in rapamycin-treated cells (Figure 6A-C). Similarly, the lysosomal marker Lamp1 showed increased colocalization with Rab5 after treatment with rapamycin (Figure 6D-F). The incorporation of later stage endocytic pathway markers suggests that the maturation of the reorganized endocytic pathway is being affected. This may be caused by an increase in merger events (similar to peroxisomes, Figure 4), a change in the motile characteristics of the compartment (as observed on short timescales with optogenetic stimulation, Figure 1), or another mechanism. Rapamycin treatment alone was demonstrated to not be sufficient to increase colocalization between these markers (Figure S2D-I in File S1). However, consistent with previous results, the myosin 6/5 chimera

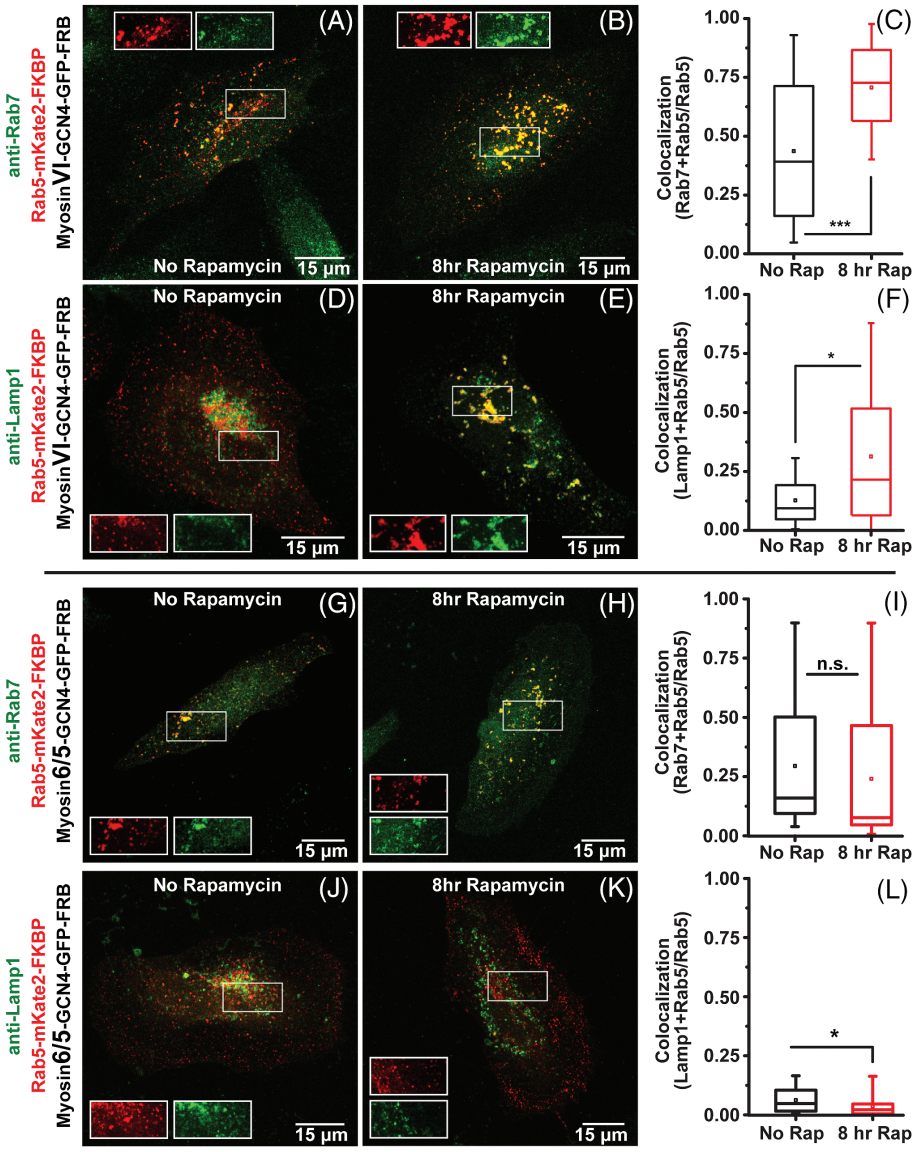

FIGURE 6 Reorganized endosomes show enhanced overlap with distinct functional markers for later stage endocytic compartments. (A, B) Colocalization of an anti-Rab7 antibody with Rab5 in untreated (A) and rapamycin-treated (B) cells co-transfected with myosin VI-GCN4-GFP-FRB. (C) Quantification of colocalization of an anti-Rab7 antibody with Rab5 ($n \geq 3$ repeats of at least 12 cells each per condition). (D, E) Colocalization of an anti-Lamp1 antibody with Rab5 in untreated (D) and rapamycin-treated (E) cells co-transfected with myosin VI-GCN4-GFP-FRB. (F) Quantification of colocalization of an anti-Lamp1 antibody with Rab5 ($n \geq 3$ repeats of at least 12 cells each per condition). (G, H) Colocalization of an anti-Rab7 antibody with Rab5 in untreated (G) and rapamycin-treated (H) cells co-transfected with myosin 6/5 chimera-GCN4-GFP-FRB after 8 hours. (I) Quantification of colocalization of an anti-Rab7 antibody with Rab5 early endosomes ($n \geq 3$ repeats of at least 12 cells each per condition). (J, K) Colocalization of an anti-Lamp1 antibody with Rab5 in untreated (J) and rapamycin-treated (K) cells co-transfected with myosin 6/5 chimera-GCN4-GFP-FRB. (L) Quantification of colocalization of an anti-Lamp1 antibody with Rab5 ($n \geq 3$ repeats of at least 12 cells each per condition). Image insets are ×1.3 magnified and are presented at the same brightness contrast settings as the image from which they are taken. For box and whisker plots: top and bottom hashes are 95th and 5th percentiles, box is 75th and 25th percentiles, line is median and middle spot is mean. Significance assessed by Student's *t* test, $^{*}P < .05$; $^{**}P < .01$; $^{***}P < .001$; n.s., not significant

was unable to affect these changes for Rab7 (Figure 6G-I) and actually caused a decrease in Lamp1 colocalization (Figure 6J-L), further supporting that directionality is an important factor in this phenomenon.

3 | DISCUSSION

The endocytic pathway is in a constant state of flux characterized by the gradual interchange of Rab GTPases and adaptor proteins during the maturation and differentiation of distinct compartments.[34] While Rabs are known to recruit both microtubule- and actin-based molecular motors to endocytic cargo,[35–37] motor activity has thus far been examined only as a transport function that does not influence compartment identity. This study demonstrates that the synthetic engagement of myosin VI motility on endosomes can influence their functional identity. While previous studies have demonstrated a link between Rab5 activity and microtubule-based motor activity,[35] this study links observations on myosin motility in cells[25,32] with the functional consequences of myosin engagement.[31]

We find that synthetic recruitment of myosin VI to early endosomes is sufficient to alter the process of early endosome (Rab5) maturation by increasing the association of later stage endocytic markers like Rab7 (late endosome) and Lamp1 (lysosome). In contrast to the previous reports that have solely examined the motile properties of subcellular compartments following motor recruitment, here we have combined optogenetic and chemical recruitment strategies to map the temporal influence of motor activity on organelle motility (seconds), morphology (minutes) and identity (hours). Our analysis across timescales suggests a model wherein the artificial engagement of a minus-end-directed myosin on early endosomes restricts microtubule-based motion, followed by the rapid condensation and disintegration of organelles, ultimately leading to reorganization of the compartment and overlap of markers that demarcate distinct endosomal compartments (Figure 7). The large number of adaptor proteins that target myosin VI to the endocytic pathway, combined with the unique motile properties of this unconventional myosin strongly suggest that it is uniquely poised to influence organelle homeostasis in the endogenous endocytic pathway. While this system is ultimately a synthetic one, relying on overexpressed proteins and exogenous localization stimuli, the broader cellular context in which the motors function is preserved.

Despite extensive evidence linking Rab GTPases to cytoskeletal motors, a direct link between myosin motors and organelle identity has remained elusive. There are several examples of Rab-mediated recruitment of myosins to organelles. Active Rab27a (GTP-bound) interacts with melanophilin to recruit myosin Va to melanosomes.[38] Rab11 and Rab11-FIP2 together interface myosin Vb to recycling endosomes, thereby controlling recycling of endocytic components to the membrane.[39] Myosin VI interacts with optineurin on the Golgi network, an interaction influenced by Rab8.[40,41] For microtubule-based motors, Rab5 activity has been shown to increase the vesicle association with the cellular microtubule network, and to stimulate the motility of endosomes in a reconstituted system.[35] In parallel, Rab activity is known to influence organelle morphology and identity in the early endosome compartment. Mutations increasing Rab5 activity, as well as constitutively active mutants of proteins upstream of Rab5 increase homotypic endosomal fusion resulting in large vesicles with markers for late endosomal and lysosomal compartments.[34,42–46] However, the effects of Rab activity on organelle morphology and identity have not been suggested to proceed through motor activity. In part, this is because maturation of endosomes can be achieved, albeit more slowly, when the microtubule network is depolymerized.[34] Furthermore, Rab localization during maturation depends on the activity of Rab-GEFs, independent of motor activity. In contrast, we show here that myosin VI engagement alters organelle identity independent of any direct effects on Rab activity.

Given that cytoskeletal motors are responsible for directed transport within the cell; motor engagement can be expected to enhance the motion of organelles. In turn, enhanced motility can spatially reposition organelles in cells, providing access to protein and membrane components that progress maturation. However, our data, in agreement with the observations of other groups, show that myosin VI engagement competitively suppresses directed diffusion on microtubules within seconds.[5] This competition between actin- and microtubule-based motility is accompanied by changes in organelle plasticity, reflected in the rapid condensation and disintegration of vesicles. Our data suggest that these changes in morphology lead to enhanced intermixing of organelle markers, thereby tuning the degree of overlap between different functional stages of the endocytic pathway. While the precise molecular mechanisms that link motor activity to identity are beyond the scope of this study, our findings clearly demonstrate an effect of cytoskeletal motor activity on shaping organelle identity, at least in an engineered system. This role may be either independent of or regulatory to the existing Rab maturation pathway.

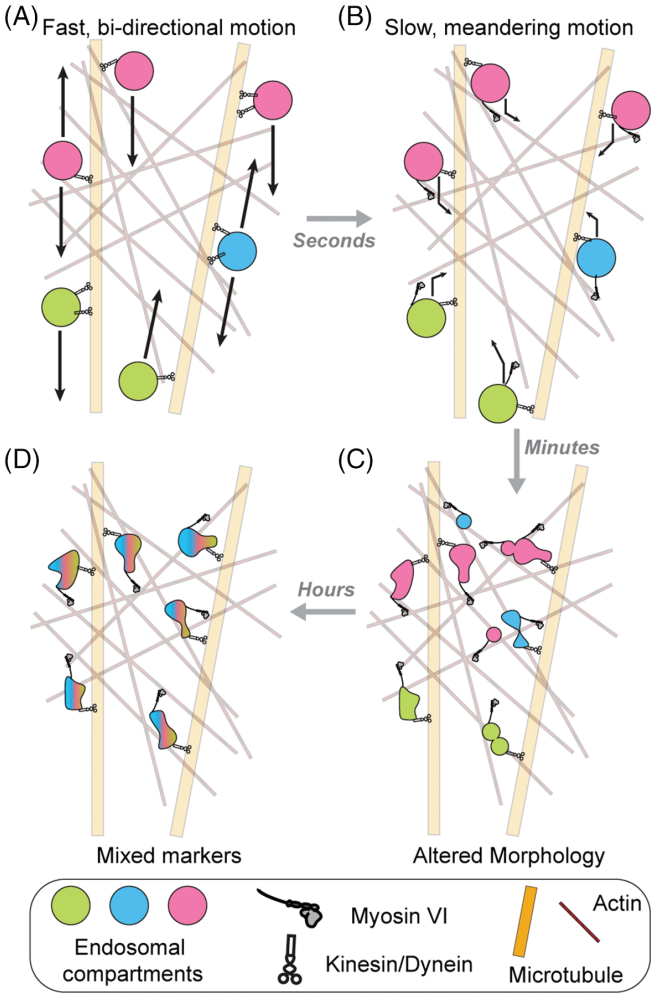

FIGURE 7 Myosin VI influences motility, morphology and identity at different timescales. (A) Endocytic motility occurs primarily on the microtubule network and features fast, bi-directional movement. (B) Upon artificial engagement of myosin VI, motility slows down and becomes less directional on a scale of seconds. (C) Over a course of minutes, myosin VI-engaged organelles begin to display altered morphology, characterized by the condensation and disintegration of vesicles. (D) After hours of myosin VI engagement, reorganization of markers conferring organelle identity is observed

Previous studies investigating myosin VI's participation in the endocytic pathway have utilized dominant negative myosin VI (cargo-binding domain) or genetic knockdowns to demonstrate the involvement of the motor at several stages of the endocytic pathway.[10,12,47] However, because of the dynamic nature of the endocytic pathway, investigating factors that influence organelle homeostasis requires

spatial and temporal control over motor activity that cannot be assessed from the complete knockdown of either motor or its cargo adaptor. Several studies have used a combination of chemical dimerization and optogenetic approaches to target motor proteins to subcellular organelles.[17–25] In this study, we have leveraged these approaches to probe the functional outcomes of myosin VI engagement in the endocytic pathway. We employ truncated versions of the myosin that should interact only with actin and the compartment-targeted dimerization partner (either FKBP or ePDZb1), thereby bypassing the native regulation of myosin VI through interactions between cargo adaptors and distinct splice variants. This strategy also controls the oligomeric state of the motor, since both monomers and dimers of myosin VI have been observed in cells.[48,49] We observed a significant rearrangement of peroxisomal cargo in cells expressing an artificially dimerized myosin construct that was less pronounced with monomeric myosin (Figure 4). Given the increased processivity of myosin dimers,[50] we reaffirm the functional importance of regulating oligomerization state in organelle homeostasis. Importantly, substantial differences in morphology based on oligomerization state were only observed for the non-native peroxisome cargo, suggesting that some cargoes may be more resilient to motile perturbations than others. Accordingly, the oligomerization state of myosin VI in distinct subcellular compartments is influenced by the unique structural regulation of the motor through the motor-cargo interaction.[48,49] Hence, while individual adaptors likely influence myosin motility through different mechanisms, our findings are not limited to a particular isoform-cargo adaptor interface. Future studies are needed to delineate the mechanisms employed by distinct myosin-cargo interfaces to influence organelle homeostasis.

4 | METHODS

4.1 | DNA constructs

Plasmids containing PEX3 (clone ID: FLH131234.01L) and Rab5a (clone ID: FLH179952.01X) were purchased from DNASU.[51] Plasmids containing mKate2 were a kind gift from Dr Daniel Schmidt (University of Minnesota). pDS275 (LOV2 domain) and pDS221 (ePDZb1) were gifts from Dr Michael Glotzer (Addgene plasmids #34972 and #34981, respectively).[26] Full-length human myosin VI containing the long insert was used as a template. Briefly, constructs were generated using restriction cloning into pcDNA5/FRT (ThermoFisher) as described below from N- to C-terminus. Myosin VI-mono-GFP-FRB contains the motor and lever-arm domains of human myosin VI (residues 1-984) followed by eGFP and FRB with 2X Gly-Ser-Gly repeats separating the domains for rotational flexibility. Myosin VI-GCN4-GFP-FRB has the same construction with addition of a GCN4 leucine zipper in between myosin VI and eGFP. Myosin V-GCN4-GFP-FRB consists of human myosin V residues M1-V1107 followed by the domains listed above in the same manner. The myosin 6/5 chimera consists of residues M1-K771 of myosin VI (comprising the motor domain, but lacking the unique insert) fused directly to residues A765-K908 of myosin V (comprising the lever arm). This construct was previously reported by Park et al[30] Variants containing the LOV2 domain are identical, however, the FRB domain has been replaced by LOV2. The myosin VI lever arm construct is the myosin VI lever arm-GCN4-GFP-LOV2 and consists of residues 814-984 containing the IQ and single alpha-helix domains of myosin VI. PEX-mKate2-FKBP consists of residues 1 to 42 of human PEX3 (sufficient for targeting[52]) followed by mKate2 and FKBP12 with no linkers between. Rab5a-mKate2-FKBP consists of FKBP12, mKate2 and full-length Rab5a. Variants containing ePDZb1 are identical; however, FKBP12 has been replaced by ePDZb1.

4.2 | Cell culture and transfection

HeLa cells (American Type Culture Collection) were cultured in DMEM supplemented with 10% FBS, 4.5 g/L D-glucose, 1% Glutamax and 20 mM HEPES, pH 7.5 and grown at 37°C, 5% CO_2. For experimental procedures, cells were plated on coverslips or glass-bottom dishes (Mattek) prior to transfection. Constructs were transfected using Lipofectamine 2000 (ThermoFisher).

4.3 | Microscopy

All images were acquired on a Nikon A1Rsi laser scanning confocal microscope with temperature, atmosphere and humidity controls (University Imaging Center). Images were acquired using a ×60 oil immersion objective (Nikon).

4.4 | Live cell imaging

Transfected cells were washed with and imaged in HEPES buffered saline (HBS, 20 mM HEPES [pH 7.4], 5 mM KCl, 14.5 mM NaCl, 2 mM $CaCl_2$, 1 mM $MgCl_2$) supplemented with 0.2% dextrose, 1 mM ascorbic acid and 1% ITS-G (Insulin, Transferrin, Selenium; ThermoFisher). Dishes were maintained at 37°C, 5% CO_2 and the appropriate relative humidity for the duration of imaging using a Tokai Hit stage top incubator. For the rapamycin labeling time course, cells were imaged immediately prior to addition of an equal volume of buffer containing 200 nM rapamycin (final concentration 100 nM) and images were acquired once every 15 minutes. For experiments using optogenetic stimulation, cells were protected from light until immediately prior to imaging. Cells of interest were located using mKate2 fluorescence to avoid activation of the LOV2 domain. Data were recorded in AVI record mode at 0.5 frames per second. Stimulation was triggered manually by activation of a 488 nm laser which also excites GFP, allowing GFP signal to be recorded. For nocodazole treatment, cells were treated with 20 μM nocodazole (1:500 dilution of dimethyl sulphoxide (DMSO) solvent, Sigma-Aldrich) for ~25 to 30 minutes at 37°C prior to imaging. Cells were imaged up to 1 hour after addition of nocodazole.

4.5 | Rapamycin treatment

Cells were washed with media and then incubated under normal culture conditions either in plain media or media-containing rapamycin (100 nM, 1:10000 dilution of DMSO solvent, Tocris). At the appropriate time point, cells were washed 3 times with phosphate buffered saline (PBS, ThermoFisher), incubated for 10 minutes with 4%

formaldehyde/PBS (ThermoFisher) at room temperature and then washed 3 times with fresh PBS. Coverslips were then mounted on slides using Prolong Diamond Anti-fade (ThermoFisher) and allowed to cure overnight at room temperature, protected from light. Slides were sealed next day with valap (Vaseline/lanolin/paraffin) and stored at 4°C when not in use. In general, slides were imaged within 1 week of fixation.

4.6 | Transferrin

Transferrin signaling was probed using Alexa-647 conjugated transferrin (ThermoFisher). Control cells and cells treated with rapamycin for 7 hours were washed with serum-free media with or without rapamycin. Cells were serum starved in this media for 1 hour. Dishes were then transferred to ice for 15 minutes. Ice-cold serum-free media containing 25 μg/mL transferrin was then added and incubated on ice for 30 minutes. Transferrin media was removed, and cells were washed with ice-cold PBS. Cells were incubated with warm serum-free media at 37°C for 10 minutes, and harvested and fixed as described above.

4.7 | Antibody labeling

Fixed cells were stored in PBS at 4°C overnight and permeabilized with 1% IGEPAL/PBS for 30 minutes at room temperature the next morning. This solution was then washed off with fresh PBS and coverslips were blocked using 1.5% normal goat serum (NGS, ThermoFisher) in PBS for 20 minutes at 37°C. Coverslips were then labeled with 1:100 Lamp1 (rabbit monoclonal, #9091S, Cell Signaling Technology) primary antibody, 1:50 Rab7 (rabbit monoclonal, #9367S, Cell Signaling Technology) primary antibody, 1:100 Rab11 (rabbit polyclonal, #715300, ThermoFisher) or 1:100 myosin VI (H-215, rabbit polyclonal, SC-50461) in PBS containing 1.5% NGS for 25 minutes at 37°C. Coverslips were dip-washed 3 times in PBS containing 0.05% TWEEN-20 (Sigma-Aldrich). Coverslips were then labeled with either 1:400 (Lamp1) or 1:200 (Rab7, Rab11, myosin VI) Alexa-647 anti-rabbit secondary $F(ab')_2$ (#4414, Cell Signaling Technology) for 25 minutes at 37°C. For co-labeling with transferrin, Rab11 was labeled with 1:200 Alexa-405 goat anti-rabbit secondary (#A31556, ThermoFisher). Coverslips were then dip-washed as above and mounted on slides as described above.

4.8 | Data analysis

Basic image analysis was done using ImageJ[53] and FIJI.[54] Particle tracking was performed in FIJI using TrackMate[55] and analysis was carried out using custom MATLAB (Mathworks) code integrating elements from the @msdanalyzer package.[56] Fixed-cell images were captured as Z-stacks and compressed to single image maximum projections. Spot size and overlap analysis were carried out using custom MATLAB code. Briefly, images of cells of interest were isolated in each channel by cropping out background regions in ImageJ. Cropped images were then automatically thresholded in MATLAB using Otsu's method to derive a threshold level as follows: Threshold = Otsu + (1-Otsu)/3. This was found to give reliable results comparable (though slightly more conservative) to hand thresholding each image. Overlapping pixels from the thresholded binary images were then counted and quantified. For spot detection, images were further analyzed by detecting the number of thresholded pixels with connectivity ≤4 and then doing a sequential addition process whereby each detected spot pixel has the value of its neighbors summed and stored as the new value for that pixel. This was iterated 10 times. Any remaining spots that had multiple centroids (eg, peroxisomes too close due to diffraction limit, projection artifacts, symmetric patterns, etc.) were then labeled by hand for each cell.

4.9 | Statistical analysis

Statistical values are presented wherever practical in figure legends. Briefly, Student's *t* test was only used when there were only 2 values calculated. All other instances use Tukey's range test for multiple comparisons with the Tukey-Kramer correction for sample sizes. Within any given data set, the single highest and lowest values are considered to be outliers and are not included in further statistical analysis.

ACKNOWLEDGMENT

This research was funded in part by NIH grants 1DP2 CA186752-01 and 5-R01-GM-105646-05 to S.S.

Conflict of interest

The authors declare no potential conflict of interest.

Editorial Process File

The Editorial Process File is available in the online version of this article.

ORCID

Sivaraj Sivaramakrishnan http://orcid.org/0000-0002-9541-6994

REFERENCES

1. Woolner S, Bement WM. Unconventional myosins acting unconventionally. *Trends Cell Biol*. 2009;19:245-252. https://doi.org/10.1016/j.tcb.2009.03.003.
2. Hartman MA, Finan D, Sivaramakrishnan S, Spudich JA. Principles of unconventional myosin function and targeting. *Annu Rev Cell Dev Biol*. 2011;27:133-155. https://doi.org/10.1146/annurev-cellbio-100809-151502.
3. Mitchison TJ. Compare and contrast actin filaments and microtubules. *Mol Biol Cell*. 1992;3:1309-1315.
4. Milo R, Phillips R. *Cell Biology by the Numbers*. New York, NY, Taylor Francis Group LLC; 2016.
5. Schroeder HW, Mitchell C, Shuman H, Holzbaur ELF, Goldman YE. Motor number controls cargo switching at actin-microtubule intersections in vitro. *Curr Biol*. 2010;20:687-696. https://doi.org/10.1016/j.cub.2010.03.024.
6. Tumbarello DA, Kendrick-Jones J, Buss F. Myosin VI and its cargo adaptors - linking endocytosis and autophagy. *J Cell Sci*. 2013;126:2561-2570. https://doi.org/10.1242/jcs.095554.
7. Wells AL, Lin AW, Chen LQ, et al. Myosin VI is an actin-based motor that moves backwards. *Nature*. 1999;401:505-508. https://doi.org/10.1038/46835.
8. Buss F, Spudich G, Kendrick-jones J. Myosin VI: cellular functions and motor properties. *Annu Rev Cell Dev Biol*. 2004;20:649-676. https://doi.org/10.1146/annurev.cellbio.20.012103.094243.

9. Wollscheid HP, Biancospino M, He F, et al. Diverse functions of myosin VI elucidated by an isoform-specific α-helix domain. *Nat Struct Mol Biol*. 2016;23:300-308. https://doi.org/10.1038/nsmb.3187.
10. Buss F, Arden SD, Lindsay M, Luzio JP, Kendrick-Jones J. Myosin VI isoform localized to clathrin-coated vesicles with a role in clathrin-mediated endocytosis. *EMBO J*. 2001;20:3676-3684. https://doi.org/10.1093/emboj/20.14.3676.
11. Morris SM, Arden SD, Roberts RC, et al. Myosin VI binds to and localises with Dab2, potentially linking receptor-mediated endocytosis and the actin cytoskeleton. *Traffic*. 2002;3:331-341. https://doi.org/10.1034/j.1600-0854.2002.30503.x.
12. Spudich G, Chibalina MV, JS A, Arden SD, Buss F, Kendrick-Jones J. Myosin VI targeting to clathrin-coated structures and dimerization is mediated by binding to disabled-2 and PtdIns(4,5)P2. *Nat Cell Biol*. 2007;9:176-183. https://doi.org/10.1038/ncb1531.
13. Reed BC, Cefalu C, Bellaire BH, et al. GLUT1CBP(TIP2/GIPC1) interactions with GLUT1 and myosin VI: evidence supporting an adapter function for GLUT1CBP. *Mol Biol Cell*. 2005;16:4183-4201. https://doi.org/10.1091/mbc.E04.
14. Bunn RC, Jensen MA, Reed BC. Protein interactions with the glucose transporter binding protein GLUT1CBP that provide a link between GLUT1 and the cytoskeleton. *Mol Biol Cell*. 1999;10:819-832. https://doi.org/10.1091/mbc.10.4.819.
15. Chibalina MV, Seaman MNJ, Miller CC, Kendrick-Jones J, Buss F. Myosin VI and its interacting protein LMTK2 regulate tubule formation and transport to the endocytic recycling compartment. *J Cell Sci*. 2007;120:4278-4288. https://doi.org/10.1242/jcs.014217.
16. Wandinger-Ness A, Zerial M. Rab proteins and the compatmentalization of the endosomal system. *Cold Spring Harb Perspect Biol*. 2014;6:a022616. https://doi.org/10.1101/cshperspect.a022616.
17. Kapitein LC, Schlager MA, van der Zwan WA, Wulf PS, Keijzer N, Hoogenraad CC. Probing intracellular motor protein activity using an inducible cargo trafficking assay. *Biophys J*. 2010;99:2143-2152. https://doi.org/10.1016/j.bpj.2010.07.055.
18. Kapitein LC, van Bergeijk P, Lipka J, et al. Myosin-V opposes microtubule-based cargo transport and drives directional motility on cortical actin. *Curr Biol*. 2013;23:828-834. https://doi.org/10.1016/j.cub.2013.03.068.
19. Esteves da Silva M, Adrian M, Schätzle P, et al. Positioning of AMPA receptor-containing endosomes regulates synapse architecture. *Cell Rep*. 2015;13:933-943. https://doi.org/10.1016/j.celrep.2015.09.062.
20. Efremov AK, Radhakrishnan A, Tsao DS, Bookwalter CS, Trybus KM, Diehl MR. Delineating cooperative responses of processive motors in living cells. *Proc Natl Acad Sci USA*. 2014;111:E334-E343. https://doi.org/10.1073/pnas.1313569111.
21. Duan L, Che D, Zhang K, Ong Q, Guo S, Cui B. Optogenetic control of molecular motors and organelle distributions in cells. *Chem Biol*. 2015;22:671-682. https://doi.org/10.1016/j.chembiol.2015.04.014.
22. Llewellyn ME, Thompson KR, Deisseroth K, Delp SL. Orderly recruitment of motor units under optical control in vivo. *Nat Med*. 2010;16:1161-1165. https://doi.org/10.1038/nm.2228.
23. Ballister ER, Ayloo S, Chenoweth DM, Lampson MA, Holzbaur ELF. Optogenetic control of organelle transport using a photocaged chemical inducer of dimerization. *Curr Biol*. 2015;25:R407-R408. https://doi.org/10.1016/j.cub.2015.03.056.
24. van Bergeijk P, Adrian M, Hoogenraad CC, Kapitein LC. Optogenetic control of organelle transport and positioning. *Nature*. 2015;518:111-114. https://doi.org/10.1038/nature14128.
25. French AR, Sosnick TR, Rock RS. Investigations of human myosin VI targeting using optogenetically controlled cargo loading. *Proc Natl Acad Sci USA*. 2017;114:E1607-E1616. https://doi.org/10.1073/pnas.1614716114.
26. Strickland D, Lin Y, Wagner E, et al. TULIPs: tunable, light-controlled interacting protein tags for cell biology. *Nat Methods*. 2012;9:379-384. https://doi.org/10.1038/nMeth.1904.
27. Granger E, McNee G, Allan V, Woodman P. The role of the cytoskeleton and molecular motors in endosomal dynamics. *Semin Cell Dev Biol*. 2014;31:20-29. https://doi.org/10.1016/j.semcdb.2014.04.011.
28. Smith JJ, Aitchison JD. Peroxisomes take shape. *Nat Rev Mol Cell Biol*. 2013;14:803-817. https://doi.org/10.1038/nrm3700.
29. Hariadi RF, Sommese R, Sivaramakrishnan S. Tuning myosin-driven sorting on cellular actin networks. *Elife*. 2015;2015:1-16. https://doi.org/10.7554/eLife.05472.
30. Park H, Li A, Chen L-Q, Houdusse A, Selvin PR, Sweeney HL. The unique insert at the end of the myosin VI motor is the sole determinant of directionality. *Proc Natl Acad Sci USA*. 2007;104:778-783. https://doi.org/10.1073/pnas.0610066104.
31. Aschenbrenner L, Lee T, Hasson T. Myo6 facilitates the translocation of endocytic vesicles from cell peripheries. *Mol Biol Cell*. 2003;14:2728-2743. https://doi.org/10.1091/mbc.E02–11.
32. Aschenbrenner L. Uncoated endocytic vesicles require the unconventional myosin, Myo6, for rapid transport through actin barriers. *Mol Biol Cell*. 2004;15:2253-2263. https://doi.org/10.1091/mbc.E04-01-0002.
33. Maxfield FR, McGraw TE. Endocytic recycling. *Nat Rev Mol Cell Biol*. 2004;5:121-132. https://doi.org/10.1038/nrm1315.
34. Rink J, Ghigo E, Kalaidzidis Y, Zerial M. Rab conversion as a mechanism of progression from early to late endosomes. *Cell*. 2005;122:735-749. https://doi.org/10.1016/j.cell.2005.06.043.
35. Nielsen E, Severin F, Backer JM, Hyman AA, Zerial M. Rab5 regulates motility of early endosomes on microtubules. *Nat Cell Biol*. 1999;1:376-382. https://doi.org/10.1038/14075.
36. Lipatova Z, Tokarev AA, Jin Y, Mulholland J, Weisman LS, Segev N. Direct interaction between a myosin V motor and the Rab GTPases Ypt31/32 is required for polarized secretion. *Mol Biol Cell*. 2008;19:4177-4187. https://doi.org/10.1091/mbc.E08-02-0220.
37. Hutagalung AH, Novick PJ. Role of Rab GTPases in membrane traffic and cell physiology. *Physiol Rev*. 2011;91:119-149. https://doi.org/10.1152/physrev.00059.2009.
38. Wu X, Wang F, Rao K, Sellers JR, Hammer JA III. Rab27a is an essential component of melanosome receptor for myosin Va. *Mol Biol Cell*. 2002;13:1735-1749. https://doi.org/10.1091/mbc.01–12.
39. Hales CM, Vaerman JP, Goldenring JR. Rab11 family interacting protein 2 associates with myosin Vb and regulates plasma membrane recycling. *J Biol Chem*. 2002;277:50415-50421. https://doi.org/10.1074/jbc.M209270200.
40. Sahlender DA, Roberts RC, Arden SD, et al. Optineurin links myosin VI to the Golgi complex and is involved in Golgi organization and exocytosis. *J Cell Biol*. 2005;169:285-295. https://doi.org/10.1083/jcb.200501162.
41. Chibalina MV, Roberts RC, Arden SD, Kendrick-Jones J, Buss F. Rab8-optineurin-myosin VI: analysis of interactions and functions in the secretory pathway. *Methods Enzymol*. 2008;438:11-24. https://doi.org/10.1016/S0076-6879(07)38002-6.
42. Rosenfeld JL, Moore RH, Zimmer KP, et al. Lysosome proteins are redistributed during expression of a GTP-hydrolysis-defective rab5a. *J Cell Sci*. 2001;114:4499-4508.
43. Hirota Y, Kuronita T, Fujita H, Tanaka Y. A role for Rab5 activity in the biogenesis of endosomal and lysosomal compartments. *Biochem Biophys Res Commun*. 2007;364:40-47. https://doi.org/10.1016/j.bbrc.2007.09.089.
44. Roberts RL, Barbieri MA, Ullrich J, Stahl PD. Dynamics of rab5 activation in endocytosis and phagocytosis. *J Leukoc Biol*. 2000;68:627-632.
45. Roberts RL, Barbieri MA, Pryse KM, Chua M, Morisaki JH, Stahl PD. Endosome fusion in living cells overexpressing GFP-rab5. *J Cell Sci*. 1999;112:3667-3675.
46. Wegener CS, Malerød L, Pedersen NM, et al. Ultrastructural characterization of giant endosomes induced by GTPase-deficient Rab5. *Histochem Cell Biol*. 2010;133:41-55. https://doi.org/10.1007/s00418-009-0643-8.
47. Masters TA, Tumbarello DA, Chibalina MV, Buss F. MYO6 regulates spatial organization of signaling endosomes driving AKT activation and actin dynamics. *Cell Rep*. 2017;19:2088-2101. https://doi.org/10.1016/j.celrep.2017.05.048.
48. Yu C, Feng W, Wei Z, et al. Myosin VI undergoes cargo-mediated dimerization. *Cell*. 2009;138:537-548. https://doi.org/10.1016/j.cell.2009.05.030.
49. Phichith D, Travaglia M, Yang Z, et al. Cargo binding induces dimerization of myosin VI. *Proc Natl Acad Sci USA*. 2009;106:17320-17324. https://doi.org/10.1073/pnas.0909748106.

50. Sivaramakrishnan S, Spudich JA. Coupled myosin VI motors facilitate unidirectional movement on an F-actin network. *J Cell Biol*. 2009;187:53-60. https://doi.org/10.1083/jcb.200906133.
51. Seiler CY, Park JG, Sharma A, et al. DNASU plasmid and PSI: biology-materials repositories: resources to accelerate biological research. *Nucleic Acids Res*. 2014;42:D1253-D1260. https://doi.org/10.1093/nar/gkt1060.
52. Kammerer S, Holzinger A, Welsch U, Roscher AA. Cloning and characterization of the gene encoding the human peroxisomal assembly protein Pex3p. *FEBS Lett*. 1998;429:53-60.
53. Schneider CA, Rasband WS, Eliceiri KW. NIH image to ImageJ: 25 years of image analysis. *Nat Methods*. 2012;9:671-675. https://doi.org/10.1038/nmeth.2089.
54. Schindelin J, Arganda-Carreras I, Frise E, et al. Fiji: an open-source platform for biological-image analysis. *Nat Methods*. 2012;9:676-682. https://doi.org/10.1038/nmeth.2019.
55. Tinevez JY, Perry N, Schindelin J, et al. TrackMate: an open and extensible platform for single-particle tracking. *Methods*. 2016;115:80-90.
56. Tarantino N, Tinevez JY, Crowell EF, et al. Tnf and il-1 exhibit distinct ubiquitin requirements for inducing NEMO-IKK supramolecular structures. *J Cell Biol*. 2014;204:231-245. https://doi.org/10.1083/jcb.201307172.

SUPPORTING INFORMATION

Additional supporting information may be found online in the Supporting Information section at the end of the article.

How to cite this article: Ritt M, Sivaramakrishnan S. Engaging myosin VI tunes motility, morphology and identity in endocytosis. *Traffic*. 2018;1–13. https://doi.org/10.1111/tra.12583